Membrane Water Treatment, *Vol. 5*, *No. 1* (*2014*) 57-*71*
DOI: http://dx.doi.org/10.12989/mwt.2014.5.1.057

Effects of slip velocity on air gap membrane distillation process

Nizar Loussif [*1,2] and Jamel Orfi [3c]

[1] *École Nationale d'Ingénieur de Monastir*, *Université de Monastir*, *Monastir*, *Tunisie*
[2] *Unité de Recherche Matériaux*, *Energie et Energies Renouvelables*,
Faculté des sciences Gafsa, *Université de Gafsa*, *2100 Gafsa*, *Tunisie*
[3] *Department of Mechanical Engineering*, *College of Engineering*, *King Saud University*, *Riyadh*, *Saudi Arabia*

(*Received August 30*, *2013*, *Revised January 20*, *2014*, *Accepted February 03*, *2014*)

Abstract. In this study, a theoretical model for the transport phenomena in an Air Gap Membrane Distillation used for desalination was developed. The model is based on the conservation equations for the mass, momentum, energy and species within the feed water solution as well as on the mass and energy balances on the membrane sides. The rarefaction impacts are taken into consideration showing their effects on process parameters particularly permeate flow and thermal efficiency. The theoretical model was validated with available data and was found in good agreement especially when the slip condition is introduced. The rarefaction impact was found considerable inducing an increase in the permeate flux and the thermal efficiency.

Keywords: water desalination; membrane distillation; air gap membrane distillation; slip velocity

1. Introduction

Membrane distillation (MD) has been widely investigated as a new technique used in desalination and water purification.

In such separation process, the driving force for desalination is the difference in vapor pressure of water caused by an existing temperature difference across the membrane. Thus, vapor molecules are transported from the high vapor pressure (high temperature) side to the low vapor pressure (low temperature) side of the membrane. This trans-membrane vapor pressure difference may be maintained with one of the four following possibilities applied on the permeate side (Rommel *et al*. 2007 and El-Bourawi *et al*. 2006):

- An aqueous solution colder than the feed solution maintained in the direct contact with the permeate side; this configuration is known as Direct Contact Membrane Distillation (DCMD).
- A cold inert gas sweeps the permeate side carrying the water vapor molecules outside the membrane module where the condensation takes place; this configuration is termed Sweeping Gas Membrane Distillation (SGMD).
- An air gap is placed between the membrane and a condensation surface; the water vapor

∗Corresponding author, Ph.D., E-mail: loussif_nizare@voila.fr

http://www.techno-press.org/?journal=mwt&subpage=7 ISSN: 2005-8624 (Print), 2092-7037 (Online)

molecules cross the membrane and the stagnant air and condense on the internal side of a cooling plate; this configuration is known as Air Gap Membrane Distillation (AGMD).

- A vacuum pump can be used to reduce the pressure in the permeate side; the condensation occurs outside of the membrane module; this configuration is termed Vacuum Membrane Distillation (VMD).

Fig. 1 describes schematically the operation principle of each MD configuration.

Exhaustive descriptions of the various physical mechanisms occurring in the MD devices can be found in (Liu *et al*. 1998, Banat and Simandel 1998, Guijt *et al*. 2005, De Pinho *et al*. 2002, Bhausaheb and Mukund 2011)).

Experimental and theoretical works have been done to show MD performance in particular the pure water production and the thermal efficiency. Previous studies which investigated MD theoretically have been interested to model heat and mass transport along MD devices. Slip velocity boundary condition was always neglected and the zero velocity at the membrane side was always considered (Alklaibi and Lior 2005, Bouguecha *et al*. 2003 and Alklaibi and Lior 2007). Besides, modeling the fluid flow with heat and mass transfer for micro-flows is different from that of the macro-scale systems. The ratio of the mean free path to characteristic length known as Knudsen number, $Kn = \lambda/L$, defines the region where the continuum assumption is valid and where it becomes no longer valid. For small values of Kn, the fluid behavior can be analyzed using the Navier Stokes equations with no-slip flow boundary conditions. For values of Kn varying between 0.001 and 0.1 the regime is called slip flow regime (Cetin *et al*. 2007). However, for Kn higher than 0.1, the continuum description is expected to fail (Hadjiconstntinou and Simek 2002).

The effect of slip flow at a membrane surface of water treatment or desalination systems was studied by few authors. Singh and Laurence (1979a, b) focused on the effect of slip velocity at the membrane surface of an ultra-filtration unit on the concentration polarization for tube and channel flow systems. The solution of the momentum and the diffusion equations for a uniform permeation rate was obtained analytically using the perturbation method. Ramon *et al*. (2009) investigated numerically the effect of slip velocity on a VMD configuration; the impact on VMD performance

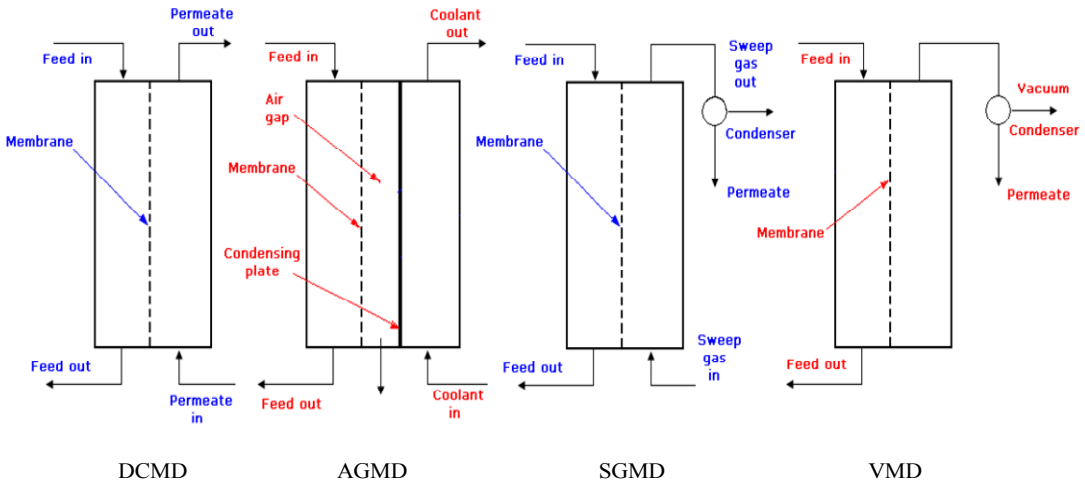

Fig. 1 Membrane distillation configurations

in terms of permeate flux and thermal efficiency was found to be significant; therefore, the degree of temperature polarization is reduced and a corresponding increase in the evaporation mass flux is observed.

The purpose of this study is to present a theoretical, two-dimensional model for the transport phenomena in the feed channel of an AGMD module including slip velocity boundary condition.

2. Mathematical model

2.1 Process description

Fig. 2 shows a description of the physical model considered in the present study. The hot saline solution flows between two parallel hydrophobic micro-porous membranes through which only water vapor can diffuse and the liquid water is retained. The vapor is condensed on the cold surface of the outer wall. An air gap is interposed between the membrane and the condensation surface. The temperature difference between the inner and the outer tubes creates a partial pressure gradient forcing the vapor to diffuse through the membrane and the air gap. The flow is symmetric along the flow direction, and so only half of the cell is shown. The calculation domain is limited to the flow, heat and mass transfer in the hot saline water region.

2.2 Governing equations

The partial differential equations governing the flow, heat and mass transfer within the hot feed water are those of conservation of mass, momentum in x and y directions, energy and species.

The following dimensionless quantities are introduced.

$$\bar{x}=\frac{x}{l}\ ,\quad \bar{y}=\frac{y}{l}\ ,\quad \bar{U}=\frac{U}{U_{in}}\ ,\quad \bar{V}=\frac{V}{U_{in}}\ ,\quad \bar{P}=\frac{P}{\rho U_{in}^2}\ ,\quad \bar{T}=\frac{T-T_c}{T_{in}-T_c}\ ,\quad \bar{C}=\frac{C}{C_{in}}$$

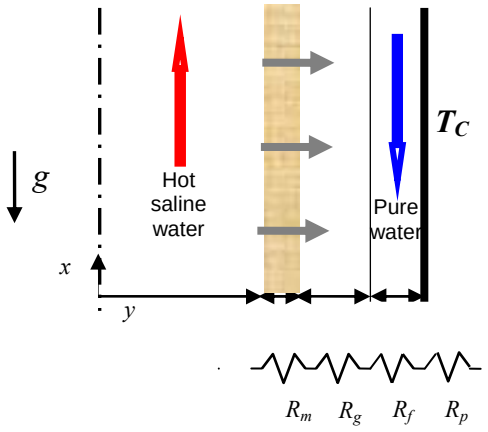

Fig. 2 Schematic diagram of an Air Gap Membrane Distillation unit (AGMD)

So we obtain

$$\frac{\partial}{\partial \bar{x}}\left(\bar{U}\right)+\frac{\partial}{\partial \bar{y}}\left(\bar{V}\right)=0 \tag{1}$$

$$\left(\overline{U}\frac{\partial \overline{U}}{\partial \overline{x}}+\overline{V}\frac{\partial \overline{U}}{\partial \overline{y}}\right)=-\frac{\partial \overline{P}}{\partial \overline{x}}+\frac{1}{\mathrm{Re}}\left[\frac{\partial^2 \overline{U}}{\partial \overline{x^2}}+\frac{\partial^2 \overline{U}}{\partial \overline{y^2}}\right] \tag{2}$$

$$\left(\overline{U}\frac{\partial \overline{V}}{\partial \overline{x}}+\overline{V}\frac{\partial \overline{V}}{\partial \overline{y}}\right)=-\frac{\partial \overline{P}}{\partial \overline{y}}+\frac{1}{\mathrm{Re}}\left[\frac{\partial^2 \overline{V}}{\partial \overline{x^2}}+\frac{\partial^2 \overline{V}}{\partial \overline{y^2}}\right] \tag{3}$$

$$\left(\overline{U}\frac{\partial \overline{T}}{\partial \overline{x}}+\overline{V}\frac{\partial \overline{T}}{\partial \overline{y}}\right)=\frac{1}{\mathrm{RePr}}\left[\frac{\partial^2 \overline{T}}{\partial \overline{x^2}}+\frac{\partial^2 \overline{T}}{\partial \overline{y^2}}\right] \tag{4}$$

$$\left(\overline{U}\frac{\partial \overline{C}}{\partial \overline{x}}+\overline{V}\frac{\partial \overline{C}}{\partial \overline{y}}\right)=\frac{1}{\mathrm{Re}Sc}\left[\frac{\partial^2 \overline{C}}{\partial \overline{x^2}}+\frac{\partial^2 \overline{C}}{\partial \overline{y^2}}\right] \tag{5}$$

The boundary conditions in dimensionless form are:
Inlet of the saline solution ($x = 0$)

$$\overline{U}=1\ ,\ \overline{V}=0\ ,\ \overline{T}=1\ ,\ \overline{C}=1 \tag{6}$$

$$\frac{\partial \overline{U}}{\partial \overline{y}}=0\ ,\frac{\partial \overline{T}}{\partial \overline{y}}=0\ ,\ \frac{\partial \overline{C}}{\partial \overline{y}}=0\ ,\ \overline{V}=0 \tag{7}$$

$$\frac{\partial \overline{U}}{\partial \overline{x}}=0\ ,\ \frac{\partial \overline{V}}{\partial \overline{x}}=0\ ,\ \frac{\partial \overline{T}}{\partial \overline{x}}=0\ ,\ \frac{\partial \overline{C}}{\partial \overline{x}}=0 \tag{8}$$

Feed saline solution - membrane interface

$$\overline{U}=-2\beta_v Kn\frac{\partial \overline{U}}{\partial \overline{y}} \tag{9}$$

$$\overline{V}=\frac{J_v}{U_{in}\rho}\ ,\ \frac{d\overline{T}}{d\overline{y}}=\frac{l\left(Q_c+Q_L\right)}{k_s\left(T_{in}-T_c\right)}\ ,\ \frac{d\overline{C}}{d\overline{y}}=\frac{J_v l}{\rho D_s C_{in}} \tag{10}$$

Where $Q_L = J_v h_{fg}$ represents the latent heat flux.

Eq. (9) respresents the boundary condition for slip velocity as described by Deissler (1964).

The vapor flux generated by the membrane will condensate on the internal side of the cooling plate, and for a thin film, the condensate film thickness δ_f can be calculated as given by Ramon *et al*. (2009) and Bejan (2004)

$$\delta_f(x) = \left(\frac{3\mu_f \int_0^x J_v(x)dx}{g\rho_f(\rho_f - \rho_v)} \right)^{1/3} \tag{11}$$

Many authors have adopted empirical approaches to describe the mass transfer across the membrane. Stephan's law is used to give the general mass flux form Alklaibi and Lior (2005)

$$J_v = K\Delta P_v \tag{12}$$

where

- J_v : Vapor flux generated by the membrane;
- K : Permeability of the membrane;
- ΔP_v : Water vapor pressure difference between the membrane sides;

The vapor pressure P_v can be calculated using the Antoine's equation

$$P_V = \exp\left(16.2620 - \frac{3799.89}{T + 226.35}\right) \tag{13}$$

The membrane permeability K is defined for the molecular diffusion as

$$K = \frac{\varepsilon D_{v/a} M_v P_T}{\chi \delta_m P_{a,moy} R_u T_{moy,m}} \tag{14}$$

Because of salt concentration, the vapor pressure at the feed side of the membrane is expressed as

$$P = (1 - C_s)P_y \tag{15}$$

Results of this work were expressed in terms of profiles of temperature, axial velocity and concentration as well as distributions of process parameters: the average permeate flux and the process thermal efficiency.

The averaged permeate flux

$$J = \frac{1}{L}\int_0^L J_v(x)dx \tag{16}$$

The averaged conduction heat flux

$$\overline{Q_C} = \frac{1}{L}\int_0^L Q_C(x)dx \tag{17}$$

The averaged total latent heat flux

$$\overline{Q_L} = \frac{1}{L}\int_0^L Q_L(x)dx \tag{18}$$

The total heat transfer

$$\overline{Q_T} = \frac{1}{L}\int_0^L Q_T(x)dx \tag{19}$$

Therefore, the process thermal efficiency can be defined as

$$\eta_t = \frac{\overline{Q_L}}{\overline{Q_T}} \tag{20}$$

Table 1 Influence of grid size on the permeate flux and the thermal efficiency

Nx, Ny	**250,40**	**350,40**	**250,50**	**350,50**
J_v **[kg/m^{2}h]**	9.4677	9.4674	9.4675	9.4672
η	0.9386	0.9379	0.9385	0.9380

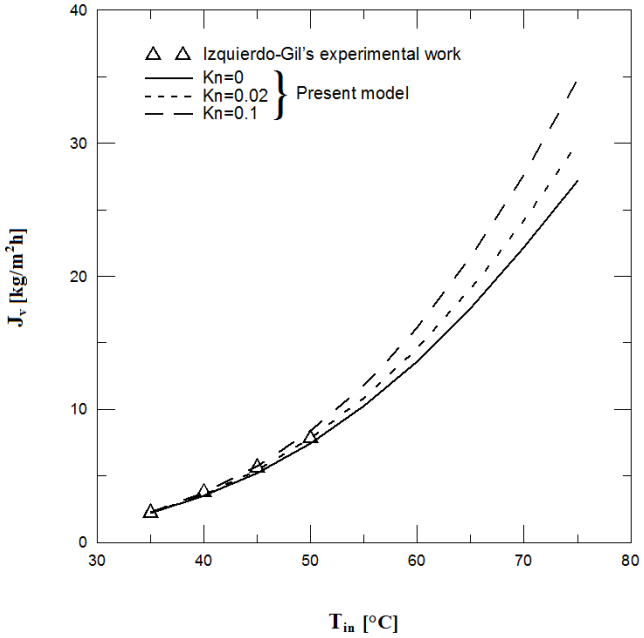

Fig. 3 Inlet temperature's effect on the permeate flux, as in this study, in comparison with the AGMD experiments of Izequierdo *et al*. (1999)

3. Numerical ethod and validation

The Control Volume Method and the Simpler algorithm (Versteeg and Malalasekera (2007)) was used for the solution. A grid-dependence analysis of the method of solution was performed as mentioned in Table 1.

The values are practically independent of the chosen grid. We select the grid size of 250,40 for the simulations conducted in this work. The computed results for AGMD were validated by comparison with Izquierdo-Gil's AGMD experimental ones (Izequierdo *et al*. 1999) and were found to be in very good agreement when considering continuum flow (Kn = 0) as shown in Fig. 3. It's important to mention that the theoretical model is enhanced when we consider slip flow model. In fact, for low temperatures, one can see that permeate flux is unchanged when varying rarefaction degrees, but when temperature increases, we can easily distinguish between different flows, due to the increase of vapor fraction near the membrane and the theoretical model based on slip model became suitable to predict experimental data.

4. Results and discussion

For all calculations, the following general conditions were considered: l = 2 mm, L = 20 cm, U_{in} = 0.15 m/s, C_{in} = 0.02; T_C = 25°C, χ =1.5; ε = 0.8; T_{in} = 75°C, δ_m = 0.4 mm, δ_g = 2 mm, δ_P = 2 mm, K_m = 0.25 W/mK, K_P = 60 W/mK.

Fig. 4 show the axial velocity profiles as function of Kn for three axial positions namely z = 3 R, z = 10 R and z = 100 R. The profiles are parabolic with a maximum velocity located at the center of the duct as it is the case for the Poiseuille flow for an impermeable channel. It's of interest to note that the effect of non zero transversal velocities did not modify the axial velocities (in

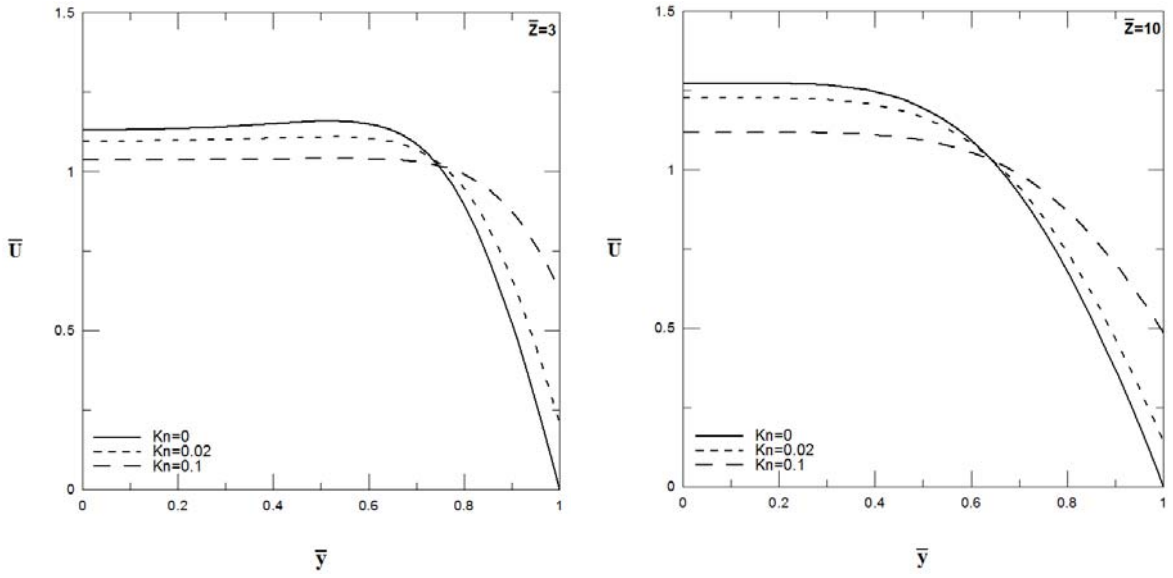

Fig. 4 Axial velocity evolutions at three axial positions and for different degrees of rarefaction

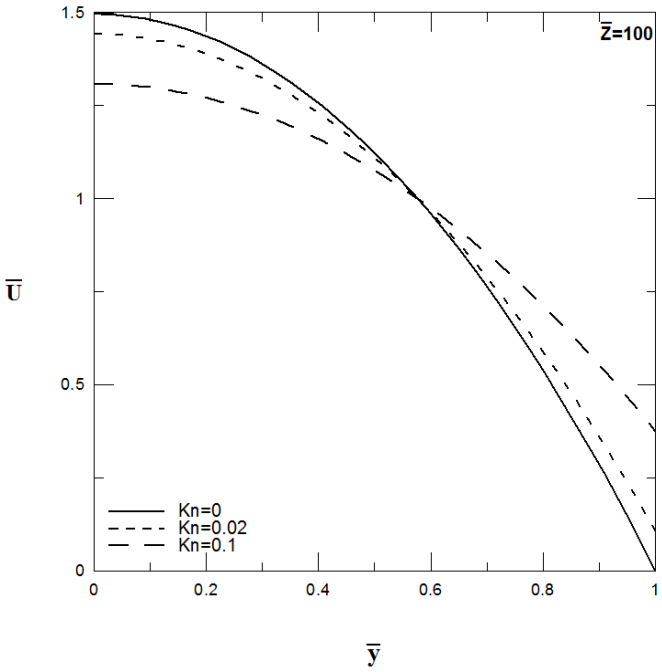

Fig. 4 Continued

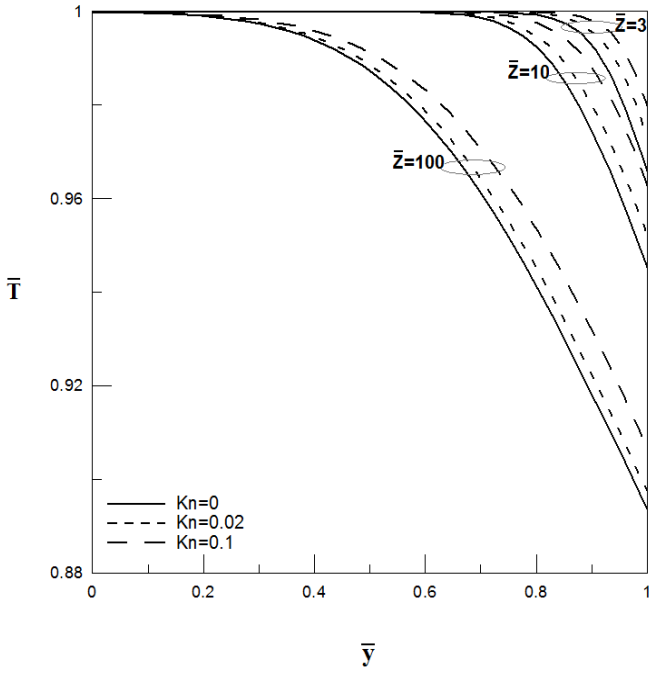

Fig. 5 Temperature evolution at three axial positions and for different degrees of rarefaction

comparison with impermeable channel) because of their low values. One can see that when the slip flow condition is applied (*Kn* is non zero), the fluid particles adjacent to the solid surface of the membrane wall no longer attain the velocity of the solid surface. In the core region of the channel, the fluid decelerates and its maximum velocity occurring at the centerline of the membrane decreases significantly. So that, increasing *Kn* leads to an increase of the fluid velocity at the membrane surface and a decrease of the centerline velocity. In fact, the resultant flow behavior is to balance the flow's mean velocity.

As mentioned in Fig. 5, the rarefaction impact on the temperature profile is significant along the duct's length. In fact, increasing *Kn* leads to a reduction of the temperature drop which allows the maintain of a higher temperature difference and the production of higher quantities of pure water.

Fig. 6 indicates the variation of salt concentration at the outlet of the duct. The concentration increases significantly near the membrane wall due to vapor loss across the membrane.

It's of interest to indicate that increasing slip velocity induces a decrease of the solution concentration near the wall surface. So that, the effect of slip coefficient is to encourage diffusive transport of solute molecules from the membrane surface to the bulk solution, and as a direct effect of this is to reduce polarization and increase permeate flux through the membrane.

Fig. 7 illustrates the variation of the process parameters (permeate flux and thermal efficiency) as a function of inlet and cooling temperature and parameterized by *Kn*. It's obvious that the presence of velocity slip increases the evaporation mass flux and the thermal efficiency. Therefore, slip effects become more pronounced at higher inlet temperatures and at lower cooling temperatures.

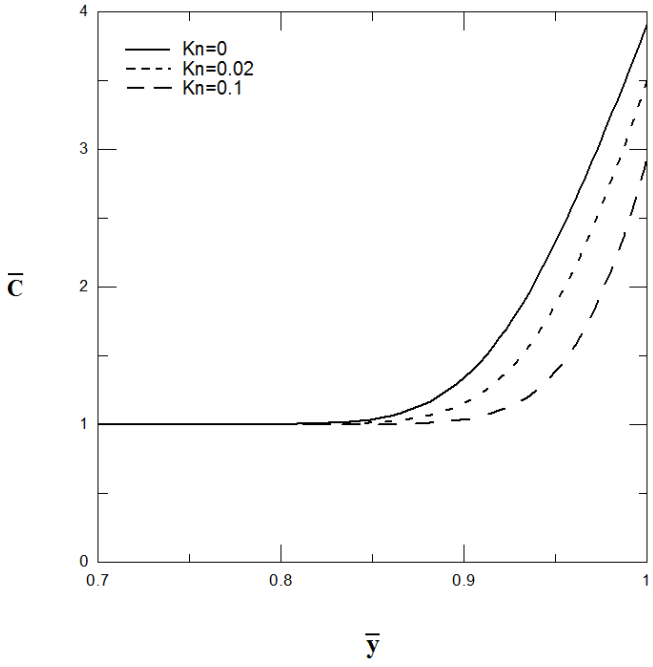

Fig. 6 Concentration evolution at the outlet of the channel as a function of Kn

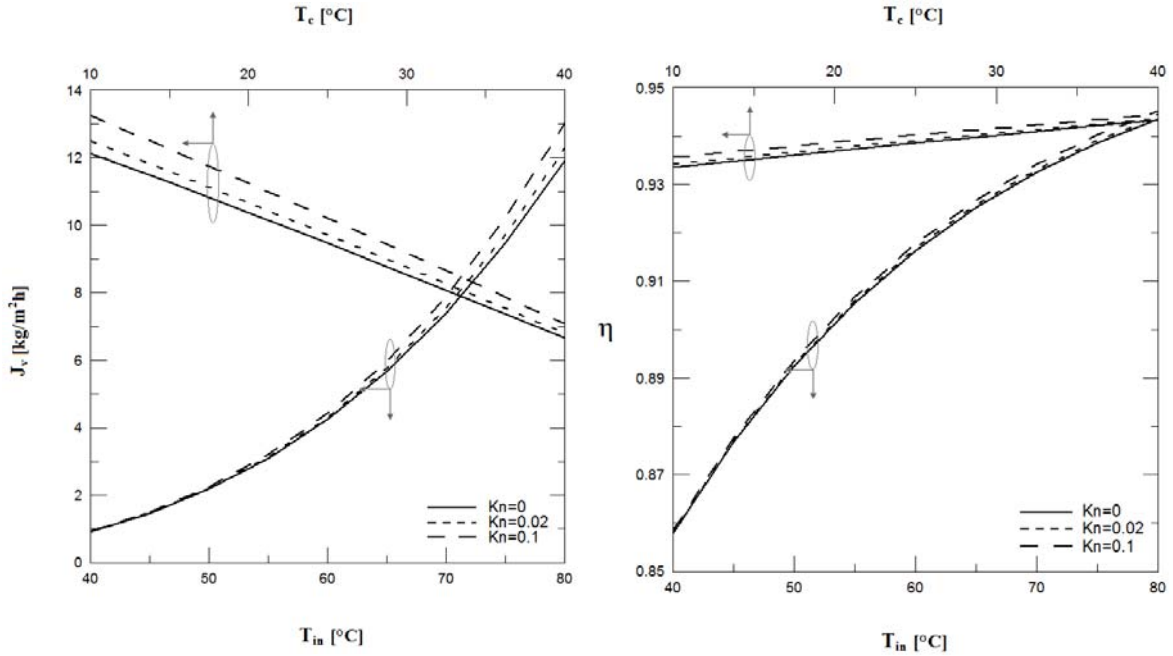

Fig. 7 Process parameters variation as a function of inlet and cooling temperatures

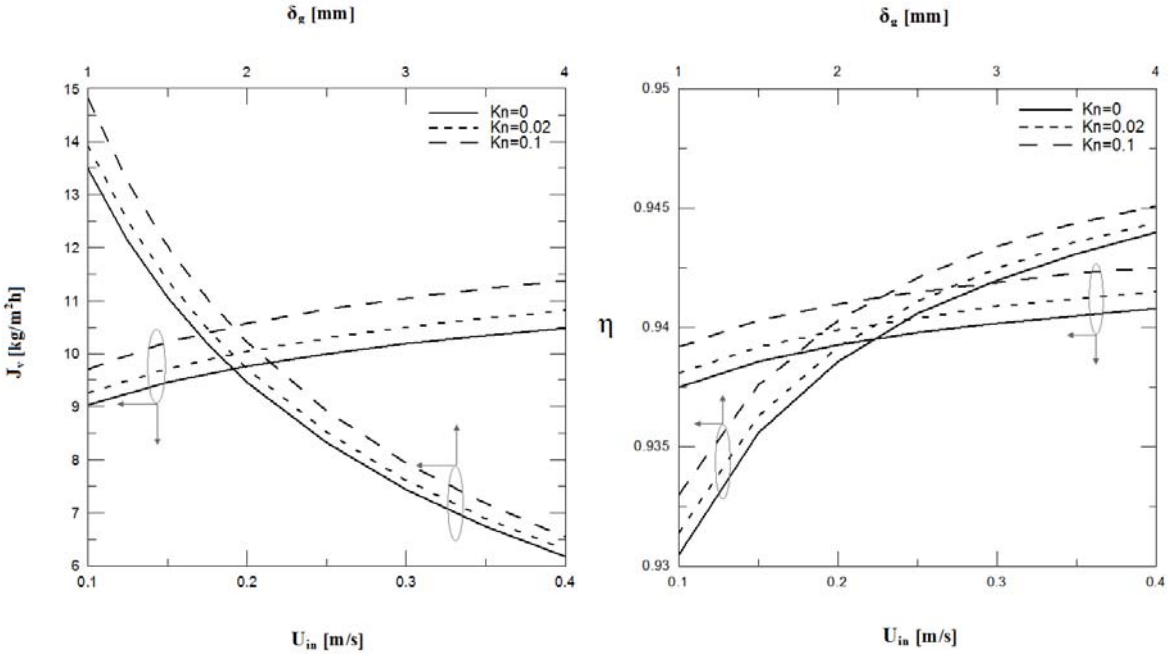

Fig. 8 Process parameters variation as a function of inlet velocity and air gap width

In fact, for T_{in} = 80°C, increasing *Kn* from zero to 0.1 induces an increase of the permeate flux, and thermal efficiency respectively by 9.25% and 0.2%.

It's of interest to note that for lower inlet temperature, the effect of rarefaction becomes insignificant.

The impacts of air gap width and the inlet velocity on process parameters are mentioned in Fig. 8. In fact, J_v and η increase with the increase of the inlet velocity, while increasing the air gap width induces a decrease of J_v and an increase of η. So that, the improvement due to increasing U_{in} is attributed to the higher velocities that reduce the *y*-direction temperature drop and maintain the driving temperature difference. The improvement due to decreasing the air gap width is because of the low thermal conductivity of the gap.

The rarefaction effect is significant. It reduces temperature drop resulting in higher production of distillated water and higher thermal efficiency as shown in all presented results.

Membrane characteristics (porosity and thermal conductivity) effects on J_v and η are presented in Fig. 9.

In fact, decreasing thermal conductivity from 0.3 to 0.1 $Wm^{-1}K^{-1}$ increases the permeate flux and the thermal efficiency respectively by 62% and 2.7%. This improvement is due to the fact that low thermal conductivity leads to low conduction heat loss and consequently more heat for vapor production.

In the other side, increasing membrane porosity from 0.7 to 0.9 induces an increase of J_v and η by 107% and 4.4% respectively. Porosity enhances process parameters because increasing ε decreases the effective thermal conductivity (i.e., conduction heat transfer) and *K* of the membrane. Moreover, in all cases, rarefaction enhances water production and thermal efficiency.

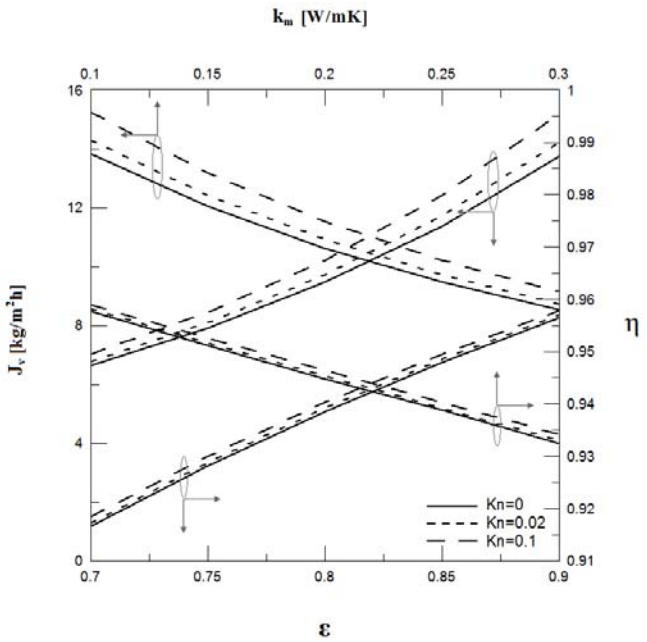

Fig. 9 Permeate flux and thermal efficiency variation as a function of membrane porosity and membrane conductivity

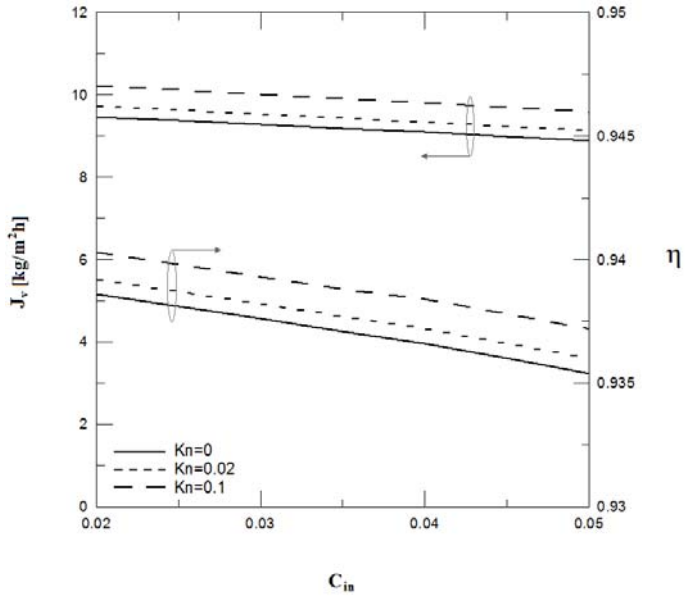

Fig. 10 Permeate flux and thermal efficiency variation as a function of inlet salt concentration

Fig. 10 shows the impact of inlet salt concentration on permeate and thermal efficiency. In fact, aqueous salt concentrations have different origins as sea water and brakish water, so that the salt concentration may have great variation and we need when proceeding to pure water production to study salt concentration effect on process parameters.

And from Fig. 10, for the continuum case, varying C_{in} from 0.02 to 0.05 induces a decrease of J_v and η respectively by 6.3% and 0.4%. As a consequence, the concentration of the inlet hot solution has a small effect on process parameters which represents an advantage of membrane distillation over pressure-driven membrane processes such as reverse osmosis in which salt concentration has important impact on process recovery ratio.

When considering rarefaction effects, J_v and η increase in comparison with the non slip case; and increasing Kn from 0 to 0.1 leads to an increase of J_v and η respectively by 7.65% and 0.2% when C_{in}= 0.05.

5. Conclusions

The slip velocity effect on the process parameters of an AGMD device are presented and discussed. Increasing rarefaction degrees leads to an increase of permeate flux and thermal efficiency. Slip effects become more pronounced at higher inlet temperatures and lower cooling temperatures. Slip flow model seems convenient for high inlet temperatures, because a low inlet temperature makes permeate flux and thermal efficiency practically unchanged.

Acknowledgments

The second author (Dr. J. Orfi) extends his appreciation to the Deanship of scientific research at King Saud University (Research group project No: RGP-VPP-091).

References

Alklaibi, A.M. and Lior, N. (2005), "Transport analysis of air gap membrane distillation", *J. Membr. Sci.*, **255**(1-2), 239-253.

Alklaibi, A.M. and Lior, N. (2007), "Comparative study of direct contact and air-gap membrane distillation processes", *Ind. Eng. Chem. Res.*, **46**(2), 584-590.

Banat, F. and Simandl, J. (1998), "Desalination by membrane distillation: A parametric study", *Sep. Sci. Technol.*, **33**(1), 201-226.

Bejan, A. (2004), *Convective Heat Transfer*, (3rd Edition), Wiley et Sons, New Jersey, USA.

Bhausaheb, L.P. and Mukund, G.S. (2011), "Heat and mass transfer analysis in air gap membrane distillation process for desalination", *Membr. Water Treat., Int. J.*, **2**(3), 159-173.

Bouguecha, S., Chouikh, R. and Dhahbi, M. (2003) "Numerical study of the coupled heat and mass transfer membrane distillation", *Desalination*, **15**(1-3), 245-252.

Cetin, B., Yuncu, H. and Kakac, S. (2007), "Gaseous flow in microconduits with viscous dissipation", *Int. J. Transp. Phenom.*, **8**(3), 297-315.

De Pinho, M., Semião, V. and Geraldes, V. (2002), "Integrated modeling of transport processes in fluid /nanofiltration membrane systems", *J. Membr. Sci.*, **206**(1-2), 189-200.

Deissler, R. (1964), "An analysis of second-order slip flow and temperature jump boundary conditions for rarefied gases", *Int. J. Heat Mass Transfer*, **7**(6), 681-694.

El-Bourawi, M.S., Ding, Z.M.R. and Khayat, M. (2006), "Framework for better understanding membrane distillation separation process", *J. Membr. Sci.*, **285**(1-2), 4-29.

Guijt, G., Meindersma, G., Reith, T. and De Haan, A. (2005), "Air gap membrane distillation: 2. Model validation and hollow performance analysis", *Sep. Purif. Technol.*, **43**(3), 245-255.

Hadjiconstntinou, N. and Simek, O. (2002), "Constant wall temperature Nusselt number in micro and nano channels", *J. Heat Transfer*, **124**(5), 356-364.

Izquierdo-Gil, M.A., Garcia-Payo, M.C. and Fernandez-Pineda, C. (1999), "Air gap membrane distillation of sucrose aqueous solutions", *J. Membr. Sci.*, **155**(2), 291-307.

Liu, G., Zhu, G., Cheung, G. and Leung, G. (1998), "Theoretical and experimental studies on air gap membrane distillation", *Heat Mass Transfer.*, **34**(1), 329-335.

Ramon, G., Agnon, Y. and Dosretz, C. (2009), "Heat transfer in vacuum membrane distillation: Effect of velocity slip", *J. Membr. Sci.*, **331**(1-2), 117-125.

Rommel, M., Koschilowski, J. and Wighaous, M. (2007), *Solar Desalination for the 21st Century*, Rizzuti *et al.*, Netherlands.

Singh, R. and Laurence, R.L. (1979a), "Influence of slip velocity at a membrane surface on ultrafiltartion performance-tube flow system", *Int. J. Heat Mass Transfer*, **22**(5) 731-737.

Singh, R. and Laurence, R.L. (1979b), "Influence of slip velocity at a membrane surface on ultrafiltration performance—II. Channel flow system", *Int. J. Heat Mass Transfer*, **22**(5), 721-729.

Versteeg, H.K. and Malalasekera, W. (2007), *An Introduction to Computational Fluid Dynamics: The Finite Volume Method*, (2nd Edition), Pearson and Prentice Hall, England.

CC

Appendix

Nomenclature

C	Mass fraction of NaCl
C_{in}	Mass fraction of NaCl at the entrance
C_p	Specific heat [$Jkg^{-1}K^{-1}$]
l	half-width of the flow channel [m]
D_s	Diffusion coefficient of NaCl [m^2/s]
$D_{v/a}$	Coefficient of vapor-air mass diffusion [m^2/s]
g	Acceleration of gravity [m/s^2]
h_{fg}	Latent heat of evaporation [J/kg]
J_V	length-averaged permeate flux at the hot side of the membrane [kg/m^2h]
J	local permeate flux at the hot side of membrane, in vapor phase [kg/m^2s]
K	permeability of the membrane
k	Thermal conductivity [W/mK]
L	Membrane length [m]
M_v	Molar mass of water vapor [$kgkmol^{-1}$]
N_x	Number of nodes along x direction
N_y	Number of nodes along y direction
P	pressure [Pa]
Pr	Prandtl number
Q_C	Conductive heat flux [kJ/m^2h]
Q_L	Latent heat flux [kJ/m^2h]
Q_T	Total flux [kJ/m^2h]
R	Universal gaz constant [J/kmol K]
Re	Reynolds number
R_g	Thermal resistance of the air gap
R_f	Thermal resistance of the condensate film
R_m	Thermal resistance of the membrane
R_p	Thermal resistance of the membrane
Sc	Schmidt number
T	temperature [°C]
U_{in}	inlet velocity [m/s]
U	axial velocity component [m/s]
V	radial velocity component [m/s]
x	Coordinate along to the solution flow [m]
y	coordinate normal to the solution flow [m]
μ	Dynamic viscosity [$kgm^{-1}s^{-1}$]

Greek Letters

v	Cinematic viscosity [m^2s^{-1}]
ρ	Density [kgm^{-3}]
ε	Porosity
χ	Tortuosity
δ	Thikness or width [m]
η	Process thermal efficiency

Subscripts

a	air
c	cooling plate
e	inlet
f	condensate film
g	air gap
P	cooling plate
m	membrane
ma	membrane material
moy	Average
s	saline solution
T	total
v	vapor